Seismic physical modeling of isotropic media based on the physical similitudes

Jose Jadsom S. de Figueiredo* (Faculty of Geophysics-UFPA and INCT-GP-Brazil), Carolina B. da Silva (Faculty of Geophysics-UFPA, Brazil), T. A. Coimbra (CEPETRO-UNICAMP-Brazil), Francisco de Oliveira (Faculty of Geophysics-UFPA, Brazil) and Leo K. Santos (Faculty of Geophysics-UFPA, Brazil)

Abstract

Most of the published works related to physical modeling use physical similitudes between model and field (geological environment) only in the geometric, and sometimes, in the kinematics sense. The dynamic similitude is approximately or, most of the time, not obeyed due to the difficulty to reproduce, in laboratory, the forces and tensions that exist inside the earth when elastic waves propagate and due to overburden (confining) pressure. In this work, we derive an analytical expression for dynamic similitude in isotropic media as a function of kinematic similitude, elastic impedance and/or through stiffness elastic tensor in the sense of dynamic stress (stress due wave propagation). The resulting expression for dynamic similitude shows that this type of similitude is a mathematically ill-posed problem and has multiple solutions in context of dynamic stress.

Introduction

There are basically three ways to generate seismic data in geophysical exploration community. The first one is the collection of seismic data from the field, a stage called seismic acquisition. In this case, there is low knowledge about the geological structures in subsurface and it is desirable to increase such knowledge through the analysis and interpretation of seismic data. The other two ways use generated synthetic data. They are called numerical modeling and physical modeling. In these cases, they need a prior knowledge about the geological model or at least a strong set of model assumptions.

A feasible seismic modeling, whether physical or computational, is a necessary tool to all stages of the seismic survey (Carcione et al., 2002). For example, the use of preliminary information on the seismic acquisition stage in a computational modeling can be used to properly configure the seismic experiment in accordance with the local geology, providing better illumination of targets of interest. In the signal processing step, such a modeler can be used to validate and adjust the methods used during this step, and finally, during the data interpretation, it can be used to compare different geological hypotheses about the model from the observed difference between predicted and existing seismic data.

In this work, we derived and applied a mathematical formalism of physical similitudes (Buckingham, 1914; Marghitu, 2001), in the context of seismic wave propagation. The main reason to do so is due to the difficulty on simulating in laboratory all geological mechanisms involved on the formation of a natural rock. The dynamic similitude is a ratio of tensions (or forces) in the field and laboratory, but in this work we derive an expression which shows this type of similitude as a function of elastic stiffness coefficients and kinematic similitude or impedance and kinematic similitude. From resulting expression for dynamic similitude, we can observe why in most of the times it is hard to take this type of similitude into account. Also, we will see that this type of similitude is an ill-posed problem. Other important issue related to the kinematic similitude is the achievement of an expression that relates the source frequency in the field with the source frequency used in laboratory.

Physical similitudes

We can define physical modeling as the ability to simulate the physical aspects of a natural scenario (large-scale) on an environment of reduced scale. In this approach, the main goal is to reproduce the behavior of the physical properties (geometric, kinematic and dynamic), displayed by a full-scale environment, in a reduced scale model (Kline, 1986). In the seismic context, more specifically in the hydrocarbon reservoir scenario, the elastic properties of the physical models reproduced in laboratory must have the highest fidelity in comparison to those shown by geological structures in the subsurface. In the following description, we will always refer to the seismic context as a field context, using the letters " f " (field) and " m " (model) to specify the full-scale and prototype environments respectively.

Geometric similitude

Generally, the scale effect of a specific phenomenon (in our case, a geologic phenomenon) increases according to the following scale ratios or scale factors (Heller, 2011) for length, area and volume,

$$\Lambda = \frac{L^{(f)}}{L^{(m)}}, \tag{1}$$

$$\Lambda^2 = \frac{(L^{(f)})^2}{(L^{(m)})^2} = \frac{A^{(f)}}{A^{(m)}}, \tag{2}$$

$$\Lambda^3 = \frac{(L^{(f)})^3}{(L^{(m)})^3} = \frac{Vol^{(f)}}{Vol^{(m)}}, \tag{3}$$

where $L^{(f)}$ is the characteristic length in the field, while $L^{(m)}$ is the corresponding length in the model. The scale

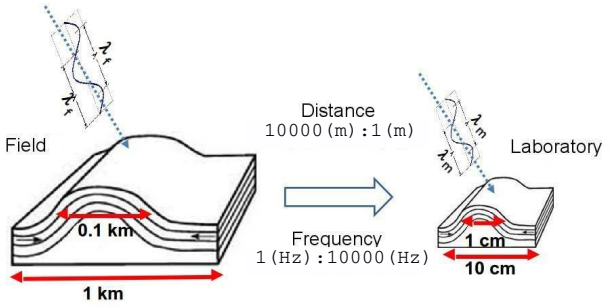

Figure 1: Seismic physical modelling in context of geometric and kinematic similitude is a result of distance upscale and frequency downscale from laboratory to field or vice versa.

factor of equation (1) in terms of proportion is defined by 1: Λ. The size of the model, time and the construction cost increase with the increasing of Λ^{-1} (Buckingham, 1914; Kline, 1986; Heller, 2011). In other words, the parameter Λ is related to the criteria of mechanic similitude called geometric similitude. Figure 1 illustrates shows how the scale change is performed from geological background to seismic physical model. An anticline structure is used as example. In the field, this kind of structure can have sizes in the order of kilometers or hundreds of meters. To model this structure in laboratory, we initially need to find the geometric similitude factor affordable to construct this model, taking into account the economic and time construction issues. In this case, an affordable scale factor between field and model would be 10000:1. Second, we need to find the better fit of seismic frequency with the ultrasonic frequency in the laboratory to perform the data acquisition. In the next section, we show that, unlike the length scale, the frequency suffers an upscale of frequency content. In the case of the example of Figure 1, the escape change is 1:10000. It means that each Hz in seismic is equivalent to 10000 Hz.

Kinematic similitude

The kinematic similitude is mathematically written by (Marghitu, 2001),

$$\Xi_V = \frac{V^{(f)}(x,y,z)}{V^{(m)}(x,y,z)} = \frac{||v^{(f)}(x,y,z)||}{||v^{(m)}(x,y,z)||} = \Xi_v \tag{4}$$

where $V^{(f)}(x,y,z)$, $V^{(m)}(x,y,z)$, $v^{(f)}(x,y,z)$ and $v^{(m)}(x,y,z)$ are the seismic velocities (interval velocities) in the field and in the model and the particle velocity in the field and in the model, respectively. It is worthy to mention that these velocities are related to the modes of vibration, P, S or converted wave velocities (in tridimensional space). From the physical point of view, equation (4) shows if the interval velocity of the model is near or far from the velocity of a geological structure that we are trying to simulate. Besides that, this ratio can also be used as a scale factor of traveltime between the real seismic section and a section from model (French, 1974).

Dynamic similitude

This type of similitude is the ratio between field forces and model forces. In the case of seismic or seismology, the effect of forces is related to the stress tensor that can be dynamic or static. Based on these behaviours, we will divide the dynamic similitude into two different approaches. First, for the static point of view, the effective stress (σ_{ij}) in a natural porous rock beneath the earth's surface is given by (Zimmerman, 1990; Carcione et al., 2003)

$$\sigma_{ij} = S_{ij} - \alpha P_{ij}^{pore} \tag{5}$$

where S_{ij}, P_{ij}^{pore} and α are the confining pressure, pore pressure and effective stress coefficient (dimensionless), respectively. According to the compressibility measurement performed by Zimmerman (1990), we can consider $\alpha \approx 1$. In this way, the dynamic similitude parameter associated to the static stress is given by

$$\Sigma_s = \frac{\sigma_{ij}^{(f)}}{\sigma_{ij}^{(m)}} = \frac{S_{ij}^{(f)} - P_{ij}^{pore(f)}}{S_{ij}^{(m)} - P_{ij}^{pore(m)}}. \tag{6}$$

In the case of low porosity rocks, the equation (6) becomes

$$\Sigma_s \approx \frac{S_{ij}^{(f)}}{S_{ij}^{(m)}}. \tag{7}$$

In expressions (6) and (7) the static dynamic similitude can be attended ($\Sigma_s = 1$) if a high pressure ultrasonic equipment is used in order to submit the sample to high confining pressure with controlled pore pressure environment. Second, now considering the dynamic similitude in the dynamic stress context, the definition of stress as a function of stiffness elastic coefficients (C_{ijkl}) and strain tensor (ε_{kl}) is given by:

$$\sigma_{ij}^{(f)} = C_{ijkl}^{(f)} \varepsilon_{kl}^{(f)}, \tag{8}$$

for field and

$$\sigma_{ij}^{(m)} = C_{ijkl}^{(m)} \varepsilon_{kl}^{(m)}, \tag{9}$$

for model.

It is known that the dynamic stiffness elastic coefficients (C_{ijkl}) depend on the velocities (P and S) as well as the density. In this way, we can see, in the dynamic point of view, that (C_{ijkl}) is dependent of kinematic properties (V_P, V_S). In other words, we have

$$C_{ijkl}^{(f)} = C_{ijkl}^{(f)}(V_P^{(f)}, V_S^{(f)}, \rho^{(f)}) \tag{10}$$

$$C_{ijkl}^{(m)} = C_{ijkl}^{(m)}(V_P^{(m)}, V_S^{(m)}, \rho^{(m)}) \tag{11}$$

where $\rho^{(f)}$ and $\rho^{(m)}$ are the rock and model densities, respectively. In the geological context, velocities and density also depend on other physical parameters, such as:

$$V_P^{rock} = V_P^{rock}(\phi, T, V_{clay}, \alpha, \sigma_{eff}) \tag{12}$$

$$V_S^{rock} = V_S^{rock}(\phi, T, V_{clay}, \alpha, \sigma_{eff}) \tag{13}$$

$$\rho^{rock} = \rho^{rock}(\rho_{matrix}, \phi, S_{fluid}) \tag{14}$$

where ϕ, T , V_{clay}, α, p_{eff}, ρ_{matrix} and S_{fluid} correspond to: porosity, temperature, clay volume, physical parameters of fracture or cracks (aspect-ratio, crack density, etc), effective pressure, matrix density (grain density) and fluid content in pores. For now we will consider the analysis of this third

type of similitude only in the context of velocity and density. Later, we will highlight these physical and petrophysical parameters that affect the velocity and density magnitude in the rocks. The demonstration of dynamic similitude for dynamic stress/strain relation is given by

$$\Sigma_d = \frac{C_{kl}^{(f)}}{C_{kl}^{(m)}} \frac{f^{(f)}V^{(m)}}{V^{(f)}f^{(m)}} \frac{\left\|u_l^{(f)}\right\|}{\left\|u_l^{(m)}\right\|}. \quad (15)$$

where $\left\|u_l^{(m)}\right\|$ and $\left\|u_l^{(m)}\right\|$ are the magnitude of particle displacement vector in the field and in the model, respectively. The particle velocity can be described as:

$$v_l = \frac{du_l}{dt} \doteq -i\omega A_0 e^{i(kx-wt)} \doteq -i\omega u_l, \quad (16)$$

where the inverse is

$$u_l = i\frac{v_l}{\omega}. \quad (17)$$

Since the value of Σ must be positive and real, it is required to get the absolute value of u_l and v_l. In this case, we have

$$\|u_l\| = \frac{\|v_l\|}{\omega} = \frac{\|v_l\|}{2\pi f}. \quad (18)$$

Replacing the value of $\|u_l\|$ in equation 15, we have

$$\Sigma_d = \frac{C_{kl}^{(f)}}{C_{kl}^{(m)}} \frac{f^{(f)}V^{(m)}}{V^{(f)}f^{(m)}} \frac{\frac{\|v_l\|^{(f)}}{2\pi f^{(f)}}}{\frac{\|v_l\|^{(m)}}{2\pi f^{(m)}}}. \quad (19)$$

Excluding the values of frequency on the equation above, we have

$$\Sigma_d = \frac{C_{kl}^{(f)}}{C_{kl}^{(m)}} \frac{V^{(m)}}{V^{(f)}} \frac{\left\|v_l^{(f)}\right\|}{\left\|v_l^{(m)}\right\|}, \quad (20)$$

or in terms of kinematic similitude

$$\Sigma_d = \frac{C_{kl}^{(f)}}{C_{kl}^{(m)}} \frac{\Xi_v}{\Xi_V}, \quad (21)$$

where Ξ_V and Ξ_v are the kinematic similitude related to the medium velocity and particle velocity, respectively. A general feature of equation (21) is that it depends only on velocities (medium and particle motion) and densities because, in this case, as mentioned before, the stiffness coefficient (C_{kl}) depends on these parameters. Other way to find a similar equation to the (21) is to use the wave equation motion derived from third Newton's law. This other similar relation is given by

$$\Sigma_d = \frac{\rho^{(f)}V^{(f)}}{\rho^{(m)}V^{(m)}} \frac{\left\|v_k^{(f)}\right\|}{\left\|v_k^{(m)}\right\|}. \quad (22)$$

As we can see, equation (22) is similar to equation (21). The only difference lies on the fact that second one is written as a function of the impedance and the kinematic similitude.

Analysis and discussions

In this section, we will discuss the more important type of similitude on physical modeling, in other words, the dynamic similitude. The geometric similitude will not be considered since it has already been contemplated in the last section.

Dynamic similitude from static stress

As mentioned above, the dynamic similitude in seismic context is divided in two types of similitudes. Regarding the external stress condition (dynamic similitude in static context), with an adequate high-pressure equipment (ultrasonic), it is possible to reach a pressure similar to the one in the subsurface. Figure 2 shows P- and S-wave velocities and density well logs from Norne field-Norway (well 660810-B-4AH) as well as the overburden stress (S_{over}) as a function of depth (z) estimated by

$$S_{over}(z) = S_{over}(z_0) + g\int_{z_0}^{z} \rho(z)dz \quad (23)$$

where g is the gravitational acceleration constant, z_0 is the initial depth and $\rho(z)$ is the density. It is worthy to

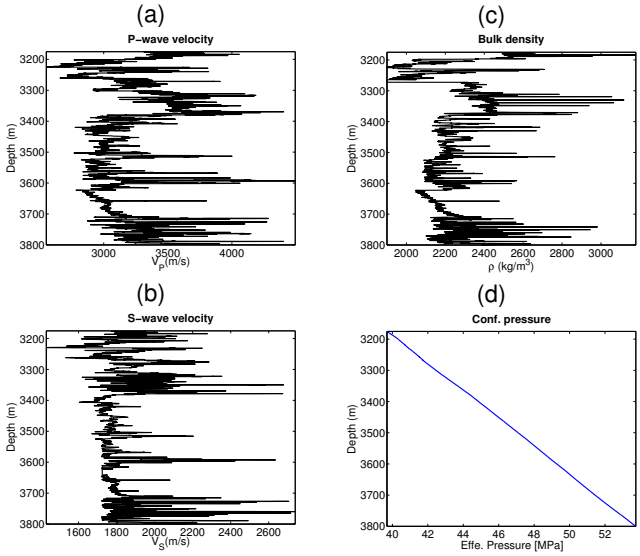

Figure 2: (a) P-wave velocity, (b) S-wave velocity and (c) density well logs from Norne field-Norway (well 660810-B-4AH). The overburden pressure (d) was calculated based on equation (23).

mention that the effective pressure expressed by equation (23) is not displayed in Figure (2 d). There are several methods used to estimate the pore pressure in a reservoir, even from seismic (Carcione et al., 2003) as well as from well-log (Zhang, 2011) datasets. As shown in equation (5), the pore-pressure tends to decrease the effective pressure. Considering this, it is correct to affirm that most of high-pressure equipments (ultrasonic) can provide enough pressure to keep a similar static stress magnitude from a great number of hydrocarbon reservoir in the field (e.g., Vernik and Nur (1992); Sun et al. (2009)).

Ill-posed problem for dynamic similitude (from dynamic stress)

In the case of isotropic media, the stiffness coefficient associated to P-wave propagation is given by,

$$C_{11} = C_{22} = C_{33} = \rho V_P^2. \tag{24}$$

In this way, we can write equation (21) for dynamic P-wave similitude as follows

$$\Sigma_d^P = \frac{C_{11}^{(f)}}{C_{11}^{(m)}} \frac{\Xi_v^P}{\Xi_V^P} = \frac{C_{11}^{(f)}}{C_{11}^{(m)}} = \frac{\rho^{(f)} V_P^{(f)2}}{\rho^{(m)} V_P^{(m)2}}. \tag{25}$$

For S-wave, the stiffness coefficient is given by

$$C_{44} = C_{55} = C_{66} = \rho V_S^2. \tag{26}$$

and consequently, the dynamic S-wave similitude is written as

$$\Sigma_d^S = \frac{C_{44}^{(f)}}{C_{44}^{(m)}} \frac{\Xi_v^S}{\Xi_V^S} = \frac{C_{44}^{(f)}}{C_{44}^{(m)}} = \frac{\rho^{(f)} V_S^{(f)2}}{\rho^{(m)} V_S^{(m)2}}. \tag{27}$$

For mixed P- and S- wave modes, we have

$$C_{12} = C_{13} = C_{23} = C_{11} - 2C_{44} = \rho(V_P^2 - 2V_S^2), \tag{28}$$

consequently, the PS dynamic similitude is given by

$$\Sigma_d^{PS} = \frac{C_{11}^{(f)} - 2C_{44}^{(f)}}{C_{11}^{(m)} - 2C_{44}^{(m)}}, \tag{29}$$

or in function of $\frac{V_P}{V_S}$ ratio

$$\Sigma_d^{PS} = \Sigma_d^S \left[\frac{\frac{V_P^{(f)2}}{V_S^{(f)2}} - 2}{\frac{V_P^{(m)2}}{V_P^{(f)2}} - 2} \right]. \tag{30}$$

Examples related to ultrasonic measurements performed in real and synthetic rocks better expresses the ambiguity exposed above. Table 1 shows the same elastic and petrophysical parameters synthetic samples of sandstones (Rathore et al., 1995; Ding et al., 2014a; Tillotson et al., 2012, 2011; Ding et al., 2014b; Berge et al., 1995). To proceed with our analysis of the ill-posed problem of dynamic similitude, on the point of view of dynamic stress, we calculated the degree of similitude between the Navajo sandstone (Berge et al., 1995) (that has $V_P = 4200$ m/s, $V_P = 2800$ m/s and $\rho = 2350\ kg/m^3$) and the synthetic sandstones shown in Table 1 for the three types of dynamic similitudes ($\Sigma_d^S \to 1, \Sigma_d^S \to 1$ and $\Sigma_d^{PS} \to 1$). Figure 3a shows that the better dynamic similitude (i. e., $\Sigma \to 1$) between real rock and synthetic rocks does not imply that all elastic parameters are similar (see Figures 3b, 3c and 3d).

Figures 3b and 3c show the kinematic similitude close to 1 (for both P- and S- wave modes), when compared to sandstone manufactured by Tillotson et al. (2011, 2012) and sample A from Berge et al. (1995). Although it has the same velocity values, the density in both cases differ by a factor of 0.3 (Tillotson et al., 2011, 2012) and 0.4 (Berge et al., 1995) related to the model density. Other important fact that can be observed in Figure 3a is the variance in uncertainty of parameter $\Sigma_d^{PS} \to 1$). This occurs because the other ratios (V_P^f/V_P^m, V_S^f/V_S^m and ρ_P^f/ρ_P^m,) are dissimilar. When the similitude of these ratios are reached, the divergence of these parameters also tends to decrease. Figure 4 shows the porosity ratio between the Sample A's porosity from Navajo Sandstone (Coyner, 1984)) and porosity from synthetic sandstones from Table 1. Again, numbers (1) to (6) mean the types of comparison. Comparison (2) does not exist because the information about porosity was not find in Ding et al. (2014a) (see **??**). In this graph, we can notice that the highest similitude in porosity (comparison-5) means highest dynamic similitude. The next highest porosity similitude is the third. Again, note that the dynamic similitude is the second closest to 1 (see Figure 3). In general, from Figure 3d and Figure 4, it is notorious that the more similar the porosity and density of an artificial rock are to a real rock, the higher the possibility of this sample to have a good dynamic similitude related to the natural rock formation.

From porosity ratio similitude, it is possible to see that porosity magnitude is an alternative to regularize the dynamic similitude for dynamic stress. In other words, the similitude in porosity (between field and model) is a priori information that can also be useful for the regularization of the ill-posed problem. The relation between density and porosity (Serra, 2008) as well as the P-wave velocity and porosity (Wyllie et al., 1956) is given by

$$\rho_{rock} = (1-\phi)\rho_{min} + \phi\rho_{fl} \Rightarrow \rho_{rock} = \rho_{min} + \phi(\rho_{fl} - \rho_{min}), \tag{31}$$

Table 1: Velocities and density values of synthetic sandstone rocks. The numbers in the first column mean where the synthetic sandstone rocks are from: 1-Rathore et al. (1995), 2-Ding et al. (2014a), 3-Tillotson et al. (2011, 2012), 4-Ding et al. (2014b), 5-Berge et al. (1995) and 6-Berge et al. (1995).

Synthetic Sandstone	Dry Vel. V_P (m/s)	Dry Vel. V_S (m/s)	Bulk Density ρ (kg/m^3)	Porosity (%)
1	2507	1575	1712	34
2	3280	2030	1427	—- *
3	4475	2710	1833	29.4
4	$\approx$ 3000 **	$\approx$ 1750 ***	1412	42
sample 1.1 5	5290	3090	2052	17.3
sample A 6	4200	2620	1710	31

* This information is not in the paper.
** Compressional-wave velocity parallel to bedding plane.
*** Shear-wave velocity parallel to bedding plane.

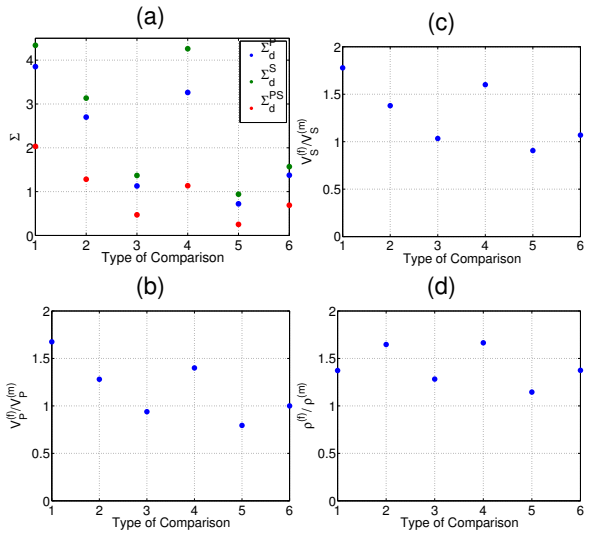

Figure 3: (a) Dynamic similitude ratio (for dynamic stress) between real elastic parameters from Navajo Sandstone (Coyner, 1984) and synthetic sandstones from (1)-Rathore et al. (1995), (2)-Ding et al. (2014a), (3)-Tillotson et al. (2011, 2012), (4)-Ding et al. (2014b), (5)-Berge et al. (1995) and (6)-Berge et al. (1995). (b) P-wave kinematic similitude, (c) S-wave kinematic similitude and (d) density ratio.

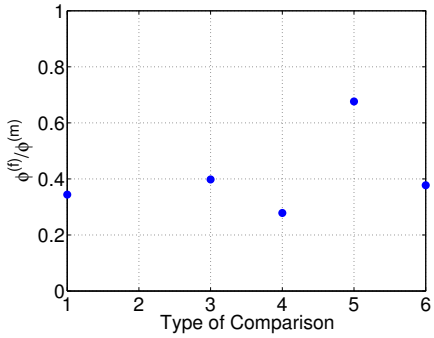

Figure 4: Porosity ratio between the porosities from Navajo Sandstone (Coyner, 1984) and synthetic sandstones from (1)-Rathore et al. (1995), (2)-Ding et al. (2014a), (3)-Tillotson et al. (2011, 2012), (4)-Ding et al. (2014b), (5)-Berge et al. (1995) and (6)-Berge et al. (1995). Comparison 2 does not exist because information about rock porosity was not find in Ding et al. (2014a).

and

$$\frac{1}{V_{rock}} = \frac{\phi}{V_{fl}} + \frac{1-\phi}{V_{min}} \Rightarrow V_{rock} = \frac{V_f V_{min}}{\phi V_{min} + (1-\phi)V_f}. \qquad (32)$$

where the terminology 'fl' and 'min' means 'fluid' and 'mineral or matrix'. It is worthy to say that this Wyllie's formulation (Wyllie et al., 1956) is valid for clean sandstone. For sandstone with porosity lower than 37 %, another equation that relates velocity with porosity is the Raymer et al. (1980)'s formulation, which mathematically is given by,

$$V_{rock} = (1-\phi)^2 V_{min} + \phi V_{fl}. \qquad (33)$$

At equations (31), (32) and (33), the rock density is linear dependent of porosity, while velocity has a non-linear dependence of porosity. These can be constraints that can reduce the ambiguity found in the dynamic similitude (from the dynamic stress point of view). Besides that, it is know that other empirical equations relating compressional and/or shear velocity with density (Gardner et al., 1974) can also be used in order to decrease the uncertainties in producing models with the same aspects of the real geological layers. Figure 5a shows the density rock as a function of porosity for a sandstone rock type (with quartz as its main mineral). For porosity range from 0 to 100 % the density interval varries from 2546 (density of quartz mineral) to 0 (air density) kg/m^3. As we can see in Figure 5a, the porosity value in the graph is close to that one from Navajo Sandstone (Coyner, 1984) ($\phi = 11.7\%$) is 11.5 %. At Figure 5a the density correspondent to 11.5 % is 2345 kg/m^3. This density value is very similar to the one of Navajo Sandstone (Coyner, 1984) ($\rho = 2350\ kg/m^3$). Figure 5b shows the estimative of P-wave velocity (bulk) versus porosity for a clean sandstone based on equations (32) and (33). The P-wave velocity of Navajo Sandstone (Coyner, 1984) is 4200 m/s, while the velocity predicted by Wyllie et al. (1956) and Raymer et al. (1980)'s equations were 4347 m/s and 2003 m/s, respectively. In this case, the prediction of bulk velocity based on Raymer et al. (1980)'s equation showed a better fit with velocity of the P-wave velocity of Navajo Sandstone (Coyner, 1984) due to the formulation itself, which was proposed for clean sandstones with porosity lower than 37 %. The estimative

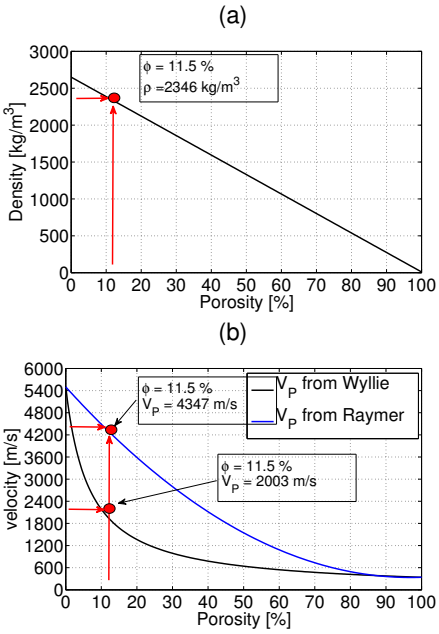

Figure 5: (a) Estimative of rock sandstone density based on equation (31). The red dot indicates the correspondent density value to the porosity of Navajo Sandstone (Coyner, 1984) . (b) Estimative of P-wave velocity (bulk) based on equations (32) and (33). The velocity values range from $5500\ m/s$ (velocity in quart) to $\approx 340\ m/s$ (air velocity). The better approximation between P-wave velocity from Navajo Sandstone (Coyner, 1984) $(4200\ m/s)$ and approximations of equation (32) and (33) was by Raymer et al. (1980)'s formulation $(4347\ m/s)$.

of rock density and velocity density in Figure 5 shows that

the similitude on porosity is an important constraint , if not the most important, to reproduce in laboratory a desirable geological structure. It is important to emphasize in both cases shown in Figure 5, it was not considered the clay content in equations (31), (32) and (33). This was due to the fact that Navajo Sandstone (Coyner, 1984) is almost a clean sandstone. When considering the percentage of clay, other generalizations with clay content correction of refereed equation should be used.

Conclusions

In this work, we performed a mathematical analysis of physical similitudes in context of experimental seismic modeling. The three physical similitudes were investigated in order to compare the similitude between a real rock formation and a synthetic seismic medium manufactured at laboratory. On the basis of our analysis, the following observations can be made:

1- According to our analysis and comparisons, the geometrical and kinematic similitude are almost always reached in laboratory environment, due to the geometrical features of geological layers that can be reproduced at laboratory and to 'some' types of material that have the same velocity of the geological layer of interest.

2- According to our analysis, the dynamic similitude (in context of dynamic stress) is a ill-posed problem. The physical consequences of this ambiguity is a remarkable feature, namely, the fact that different density with different velocity values around the exact value may present the same elastic stiffness coefficients.

3- The porosity control is a preponderant constraint in order to reach a suitable similitude between real and manufactured synthetic rocks on a dynamic stress point of view. Other priori informations (by using empirical equation), such as formation temperature, clay volume content, porosity and effective pressure formation can be used in the regularization of this ill-posed problem. In the petrophysical point of view, the difficult is to create a rock with density and velocities (P and S) similar to those that the earth possess. This difficulty is the main reason why, most of the times, the dynamic similitude is an ill-posed problem

Acknowledgments

We would like to thank NTNU-Norway for kindly providing the well-logs data. The authors also would like to thank CAPES, INCT-GP and CNPq from Brazil and the graduate program at Federal University of Pará for the financial support in this research.

References

Berge, P. A., B. P. Bonner, and J. G. Berryman, 1995, Ultrasonic velocity-porosity relationships of sandstone analogs made from fused glass beads: Geophysics, **60**, 108–119.

Buckingham, E., 1914, On physically similar systems; illustrations of the use of dimensional equations: Physics Review, **4**, 345–376.

Carcione, J., H. Helle, N. Pham, and T. Toverud, 2003, Pore pressure estimation in reservoir rocks from seismic reflection data: GEOPHYSICS, **68**, 1569–1579.

Carcione, J. M., G. C. Herman, and A. P. E. ten Kroode, 2002, Seismic modeling: Geophysics, **67**, 1304–1325.

Coyner, K. B., 1984, Effects of stress, pore pressure, and pore fluids on bulk strain, velocity, and permeability in rocks: Thesis, Massachusetts Institute of Technology. (Thesis (Ph.D.)–Massachusetts Institute of Technology, Dept. of Earth, Atmospheric and Planetary Sciences, 1984.).

Ding, P., B. Di, D. Wang, J. Wei, and X. Li, 2014a, P and s wave anisotropy in fractured media: Experimental research using synthetic samples: Journal of Applied Geophysics, **109**, 1–6.

Ding, P., B. Di, J. Wei, X. Li, and Y. Deng, 2014b, Fluid-dependent anisotropy and experimental measurements in synthetic porous rocks with controlled fracture parameters: Journal of Geophysics and Engineering, **11**, 015002.

French, W., 1974, Twoâdimensional and threeâdimensional migration of modelâexperiment reflection profiles: GEOPHYSICS, **39**, 265–277.

Gardner, G., L. Gardner, and A. Gregory, 1974, Formation velocity and density—the diagnostic basics for stratigraphic traps: GEOPHYSICS, **39**, 770–780.

Heller, V., 2011, Scale effects in physical hydraulic engineering models: Journal of Hydraulic Research, **49**, 293–306.

Kline, J. S., 1986, Similitude and approximation theory: Springer-Verlag.

Lindseth, R., 1979, Synthetic sonic logs—a process for stratigraphic interpretation: GEOPHYSICS, **44**, 3–26.

Marghitu, D. B., 2001, Mechanical engineer's handbook: Academic Press.

Rathore, J. S., E. Fjaer, R. M. Holt, and L. Renlie, 1995, P- and S-wave anisotropy of a synthetic sandstone with controlled crack geometry: Geophysical Prospecting, **43**, 711–728.

Raymer, L. L., E. R. Hunt, and J. S. Gardner, 1980, An improved sonic transit time-to-porosity transform: 21st Annual Logging Symposium Transactions, 1–13.

Serra, O., 2008, Well Logging Handbook: Editions OPHRYS.

Sun, M., D. Han, and M. Batzle, 2009, CO2 velocity measurements and models for temperatures down to -10°c and up to 200°c and pressures up to 100 MPa, *in* SEG Technical Program Expanded Abstracts 2009: Society of Exploration Geophysicists, SEG Technical Program Expanded Abstracts, 2090–2094.

Tillotson, P., M. Chapman, A. I. Best, J. Sothcott, C. McCann, W. Shangxu, and X.-Y. Li, 2011, Observations of fluid-dependent shear-wave splitting in synthetic porous rocks with aligned penny-shaped fractures: Geophysical Prospecting, **59**, 111–119.

Tillotson, P., J. Sothcott, A. I. Best, M. Chapman, and X.-Y. Li, 2012, Experimental verification of the fracture density and shear-wave splitting relationship using synthetic silica cemented sandstones with a controlled fracture geometry: Geophysical Prospecting, **60**, 516–525.

Vernik, L., and A. Nur, 1992, Ultrasonic velocity and anisotropy of hydrocarbon source rocks: GEOPHYSICS, **57**, 727–735.

Wyllie, M., A. Gregory, and L. Gardner, 1956, Elastic wave velocities in heterogeneous and porous media: GEOPHYSICS, **21**, 41–70.

Zhang, J., 2011, Pore pressure prediction from well logs: Methods, modifications, and new approaches: Earth-Science Reviews, **108**, 50–63.

Zimmerman, R. W., 1990, Compressibility of sandstones: Elsevier.